Use of the Bethe equation for inner-shell ionization by electron impact

Cedric J. Powell,[1] Xavier Llovet,[2] and Francesc Salvat[3]
[1]*Materials Measurement Science Division, National Institute of Standards and Technology, Gaithersburg, Maryland 20899-8370, USA*
[2]*Centres Científics i Tecnològics, Universitat de Barcelona, Lluís Solé i Sabarís 1-3, 08028 Barcelona, Spain*
[3]*Facultat de Física (ECM and ICC), Universitat de Barcelona, Diagonal 645, 08028 Barcelona, Spain*

(Received 23 February 2016; accepted 25 April 2016; published online 13 May 2016)

We analyzed calculated cross sections for K-, L-, and M-shell ionization by electron impact to determine the energy ranges over which these cross sections are consistent with the Bethe equation for inner-shell ionization. Our analysis was performed with K-shell ionization cross sections for 26 elements, with L-shell ionization cross sections for seven elements, L_3-subshell ionization cross sections for Xe, and M-shell ionization cross sections for three elements. The validity (or otherwise) of the Bethe equation could be checked with Fano plots based on a linearized form of the Bethe equation. Our Fano plots, which display theoretical cross sections and available measured cross sections, reveal two linear regions as predicted by de Heer and Inokuti [in *Electron Impact Ionization*, edited by T. D. Märk and G. H. Dunn, (Springer-Verlag, Vienna, 1985), Chap. 7, pp. 232–276]. For each region, we made linear fits and determined values of the two element-specific Bethe parameters. We found systematic variations of these parameters with atomic number for both the low- and the high-energy linear regions of the Fano plots. We also determined the energy ranges over which the Bethe equation can be used. *Published by AIP Publishing.*
[http://dx.doi.org/10.1063/1.4948700]

I. INTRODUCTION

Cross sections for ionization of inner-shell electrons in neutral atoms by electron impact are needed in many branches of physics, including atomic physics, plasma physics, radiation physics, materials analysis by electron-probe microanalysis (EPMA), surface analysis by Auger-electron spectroscopy (AES), and thin-film analysis by electron energy-loss spectroscopy. These cross sections are often used in Monte Carlo simulations to predict, for example, radiation transport in matter and the generation of X-ray and Auger-electron signal intensities in EPMA and AES.

In 1930, Bethe[1] developed a non-relativistic asymptotic expression for the cross section, per atom, for ionization of shell i in the form

$$\sigma_i = \frac{\pi e^4}{E}\frac{Z_i b_i}{E_i}\ln\left[\frac{c_i E}{E_i}\right], \tag{1}$$

where $E = mv^2/2$ is the kinetic energy of the incident electrons, v is the electron velocity, E_i is the binding energy of electrons in shell i, Z_i is the number of electrons in that shell, and e and m are the electronic charge and mass, respectively. The parameters b_i and c_i in Eq. (1) are given by

$$b_i = E_i M_i^2/Z_i \tag{2}$$

and

$$\ln\left(\frac{c_i mc^2}{2E_i}\right) = \frac{C_i}{M_i^2}, \tag{3}$$

where c is the velocity of light. The term M_i^2 in Eqs. (2) and (3) is the square of the total dipole-matrix element for ionizing collisions while the term C_i in Eq. (3) is given by an integral of the generalized oscillator strength for inner-shell ionization.[2] The parameter b_i was estimated by Bethe (using hydrogenic wave functions) to be between 0.2 and 0.6 for inner shells and, for a given shell, to be a function of atomic number, Z. The parameter c_i was estimated by Bethe to be about 4. Equation (1) was derived with use of the first Born approximation and is expected to be valid when $E \gg E_i$ and when the average energy transfer in the ionizing collision is much less than E.[2] A relativistic version of Eq. (1), given as Eq. (4) below, was published by Fano.[3]

Despite the wide use of Eq. (1) and its relativistic counterpart for estimating cross sections for inner-shell ionization, there is limited knowledge of the Bethe parameters b_i and c_i and of the energy ranges over which these equations can be expected to be valid. Powell[4–6] reported values of the Bethe parameters from fits to measured cross sections for inner-shell ionization, but the resulting parameter values were of necessity limited to the elements and energy ranges for which measurements were available.

We report a new analysis to determine the ranges of incident energy over which the Bethe equation is valid and the corresponding values of the Bethe parameters b_i and c_i. We make use of cross sections for K-, L-, and M-shell ionization that were calculated by Bote *et al.*[7,8] using a composite algorithm that combines the distorted-wave and plane-wave Born approximations. Llovet *et al.*[9] recently reviewed these calculated cross sections and the available measured cross sections. They identified elements for which there were at least three (for K shells) or two (for L and M subshells) mutually consistent sets of cross-section measurements and for which the cross sections varied with energy as expected by theory; these selections were referred to as superior values. Llovet *et al.*

found that the overall average root-mean-square deviation between the calculated cross sections and the selected measured values was 10.9% and the overall average deviation was −2.5%. This degree of agreement was considered to be very satisfactory given the difficulties of making absolute cross-section measurements.[9]

A simple but valuable method of analyzing sets of cross-sections for inner-shell ionization (or indeed any other inelastic-scattering cross sections[10]) is the Fano plot.[2–6,10] As suggested by the non-relativistic Bethe equation [Eq. (1)], a Fano plot is made by plotting $\sigma_i E E_i$ (e.g., from a set of measured or calculated cross sections over a particular energy range) versus $\ln(E/E_i)$; as we will see, a similar type of plot can be made based on the relativistic Bethe equation. If such a plot is judged to be linear, we can conclude that the data set is consistent with the Bethe equation and derive values of the Bethe parameters.[4–6] However, de Heer and Inokuti[11] have pointed out that Fano plots should display *two* linear regions if the energy range for the data set is sufficiently large. At relatively low energies, one linear region is found typically beginning at several times the threshold energy for inner-shell ionization, E_i.[4] Another linear region is expected at higher energies with a smaller slope that occurs in what is termed the asymptotic Bethe region.

The cross sections for K-, L-, and M-shell ionization that were calculated by Bote *et al.*[7,8] extend from the threshold energy for ionization to 100 GeV. The large energy range for these cross sections is thus well suited for a more

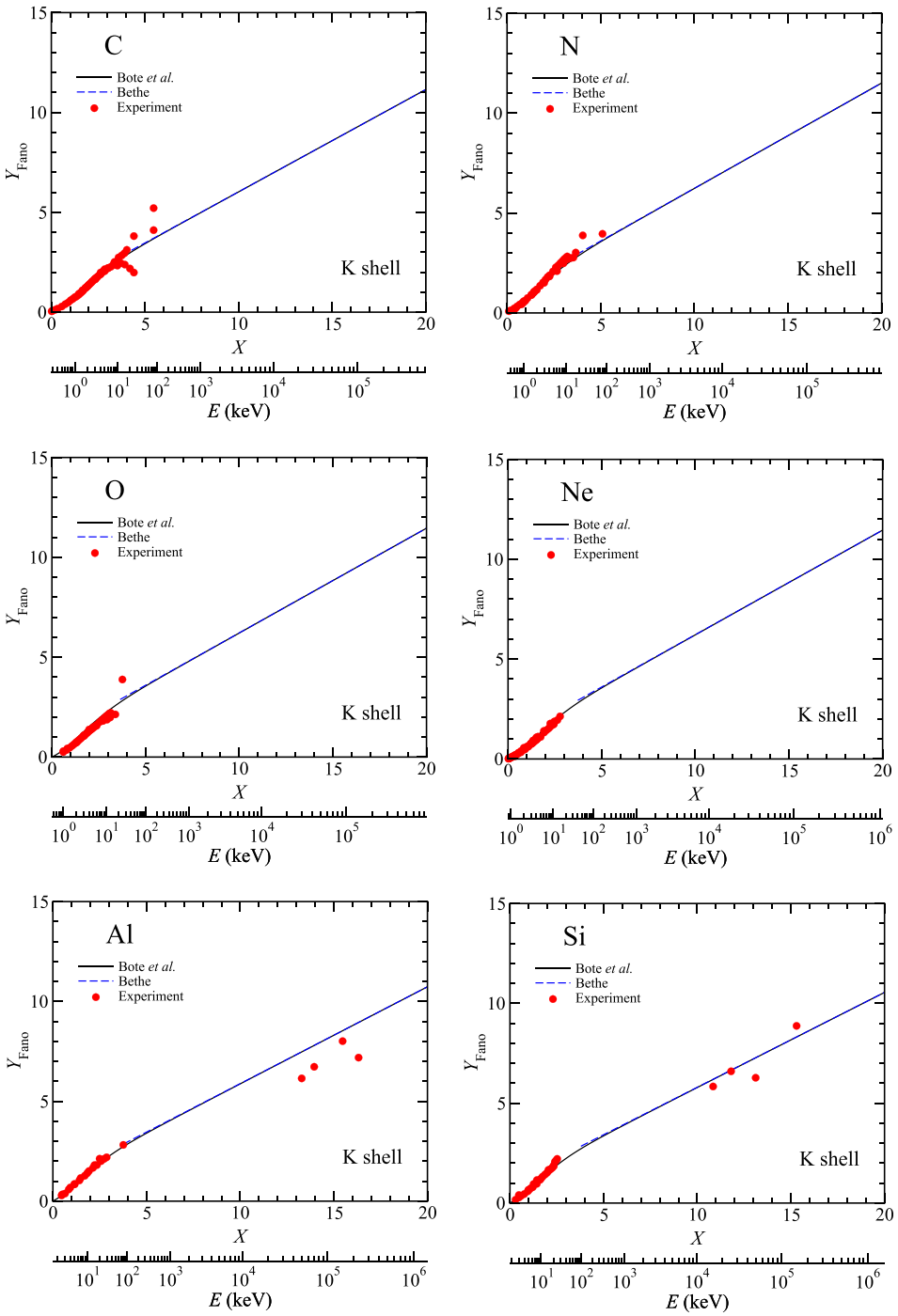

FIG. 1. Fano plots for C, N, O, Ne, Al, and Si (solid lines) based on K-shell ionization cross sections calculated by Bote *et al.*[7,8] in which Y_{Fano} from Eq. (7) is plotted against X from Eq. (6). The abscissa also shows the electron kinetic energy, E. The dashed lines show linear fits to the Y_{Fano} values from the calculated cross sections with Eq. (8) in the asymptotic high-energy region of the Fano plots. The dashed lines have been extrapolated to a lower energy at which the deviation from the solid lines is 5%. The solid circles show values of Y_{Fano} calculated from the preferred measured K-shell ionization cross sections of Llovet *et al.* (Tables 2 and 7 of Ref. 9).

extensive analysis of the Bethe equation based on Fano plots. Llovet *et al.*[9] identified 26 elements (C, N, O, Ne, Al, Si, Ar, Ca, Ti, Cr, Mn, Fe, Ni, Cu, Zn, Ga, Ge, Se, Y, Pd, Ag, Sn, Sb, Au, Pb, and Bi) with measured K-shell ionization cross sections that satisfied their selection criteria. They similarly identified seven elements (Ag, Sn, Sm, Ta, Pb, Bi, and U) with satisfactory measurements of total L-shell ionization cross sections and one element (Xe) with satisfactory measurements of L_3-subshell ionization cross sections. Finally, Llovet *et al.* identified three elements (Au, Pb, and Bi) that had satisfactory measurements of total M-shell ionization cross sections. We present Fano plots for each of these elements based on the calculated ionization cross sections. These plots clearly show the existence of two distinct linear regions, and we derive values of the Bethe parameters for each linear region. We then show systematic variations of the derived Bethe parameters with atomic number for the two linear regions and systematic differences in the Bethe parameters for K-, L-, and M-shell ionization.

II. THE FANO PLOT

The relativistic form of the Bethe equation for inner-shell ionization is[2,3]

$$\sigma_i = \frac{2\pi e^4}{mv^2}\frac{Z_i b_i}{E_i}\left\{\left[\ln\left(\frac{\beta^2}{1-\beta^2}\right)-\beta^2\right]+\ln\left(\frac{c_i mc^2}{2E_i}\right)\right\}, \quad (4)$$

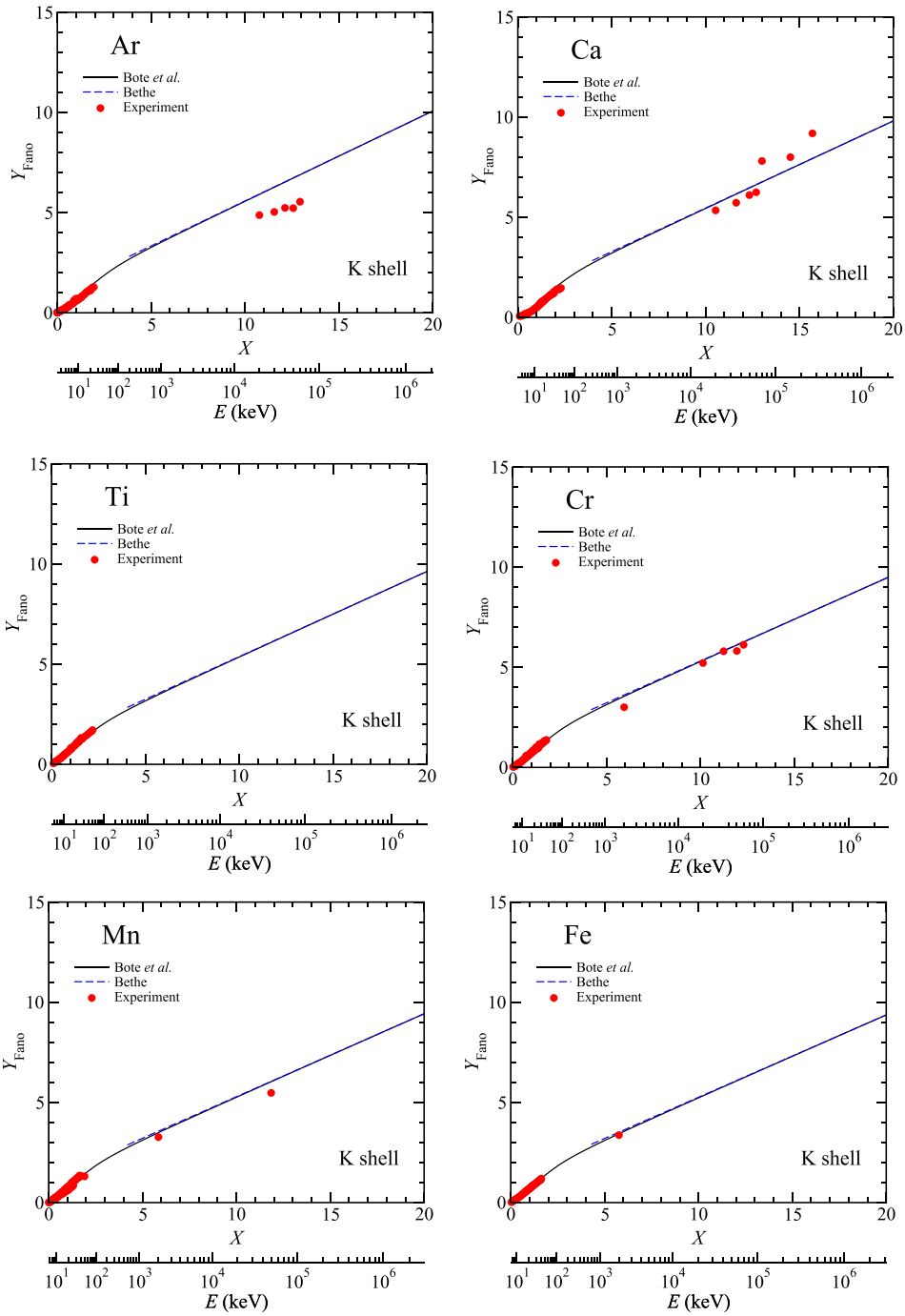

FIG. 2. Fano plots for Ar, Ca, Ti, Cr, Mn, and Fe; see caption to Fig. 1.

where β is the ratio of the electron velocity to the velocity of light, c. It is convenient to rewrite Eq. (4) as

$$\sigma_i = \frac{2\pi e^4}{mv^2}\frac{Z_i b_i}{E_i}(X + \ln c_i) = \frac{2\pi e^4}{mv^2} M_i^2 (X + \ln c_i), \quad (5)$$

where

$$X = \left[\ln\left(\frac{\beta^2}{1-\beta^2}\right) - \beta^2\right] + \ln\left(\frac{mc^2}{2E_i}\right). \quad (6)$$

A Fano plot is prepared by plotting

$$Y_{\text{Fano}} = \frac{\sigma_i m v^2 E_i}{2\pi e^4 Z_i} \quad (7)$$

versus X as suggested by Eq. (5). For linear regions of the Fano plot,

$$Y_{\text{Fano}} = b_i(X + \ln c_i). \quad (8)$$

The Bethe parameter b_i is the slope of the linear region of the plot, and the parameter c_i is determined by the ordinate at $X = 0$, where $Y_{\text{Fano}} = b_i \ln c_i$. In the nonrelativistic limit, $X \approx \ln(E/E_i) = \ln U$ and $mc^2\beta^2 \approx 2E$ where $U = E/E_i$ is the overvoltage and E is the electron kinetic energy. Equation (7) then becomes

$$Y_{\text{Fano}} = \frac{\sigma_i E_i^2 U}{\pi e^4 Z_i} = \frac{\sigma_i E E_i}{\pi e^4 Z_i}. \quad (9)$$

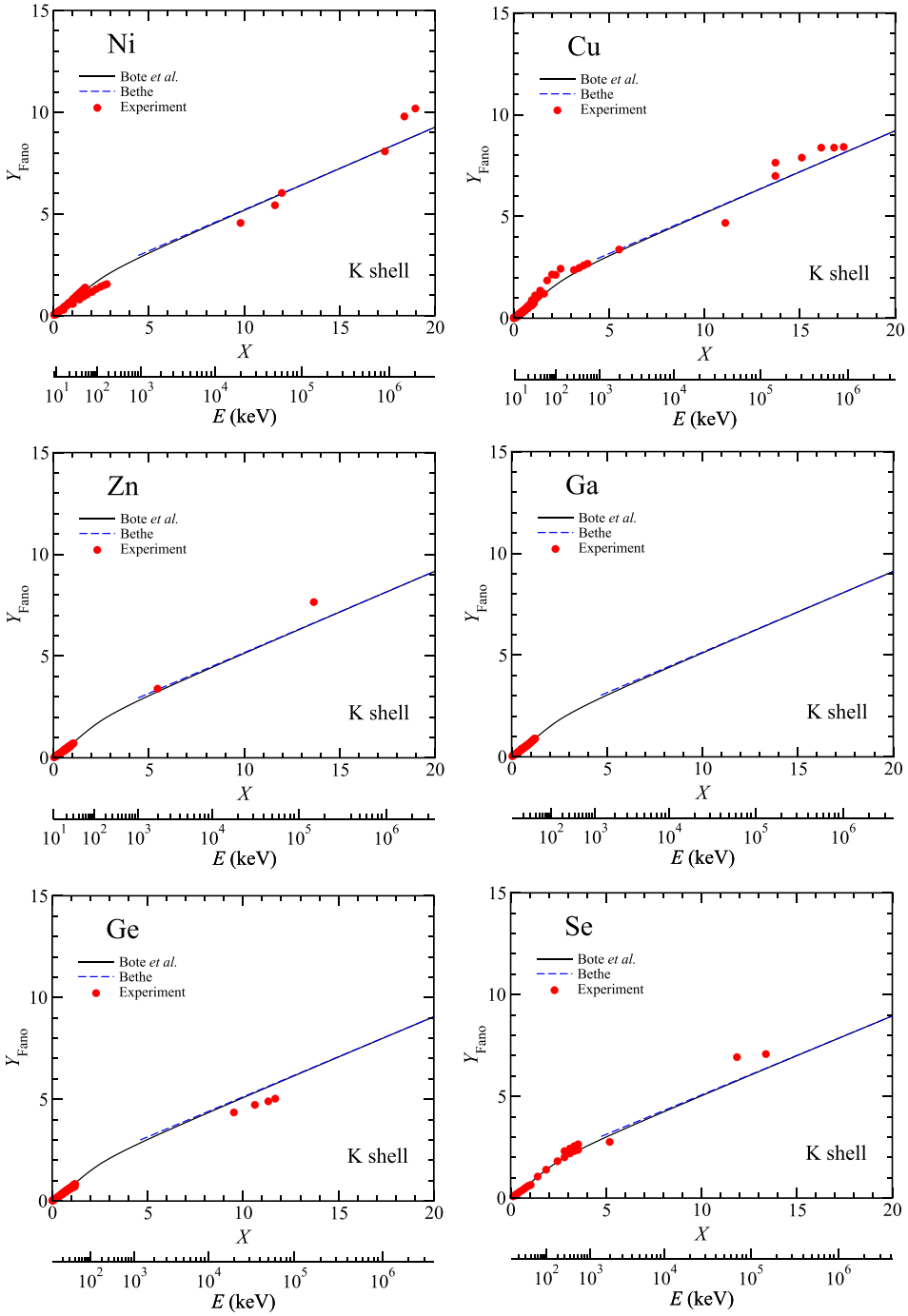

FIG. 3. Fano plots for Ni, Cu, Zn, Ga, Ge, and Se; see caption to Fig. 1.

For ionization of L and M shells, we need to determine appropriate values of E_i and Z_i depending on whether particular or all subshells contribute to the relevant ionization process. For ionization of all L subshells, for example, we have

$$M_{\mathrm{L}}^2 = \sum_{j=1}^{3} M_{\mathrm{L}j}^2 \tag{10a}$$

and

$$\ln c_{\mathrm{L}} = \frac{1}{M_{\mathrm{L}}^2} \sum_{j=1}^{3} M_{\mathrm{L}j}^2 \ln c_{\mathrm{L}j}, \tag{10b}$$

where $M_{\mathrm{L}j}^2$ is the total dipole-matrix element squared for ionization of L-subshell j and $c_{\mathrm{L}j}$ is the corresponding value of the parameter c_i. The total number of electrons in the L shell is

$$Z_{\mathrm{L}} = \sum_{j=1}^{3} Z_{\mathrm{L}j} = 8 \tag{11a}$$

and the average L-shell binding energy, $\overline{E_{\mathrm{L}}}$, is

$$\overline{E_{\mathrm{L}}} = \frac{1}{Z_{\mathrm{L}}} \sum_{j=1}^{3} Z_{\mathrm{L}j} E_{\mathrm{L}j}, \tag{11b}$$

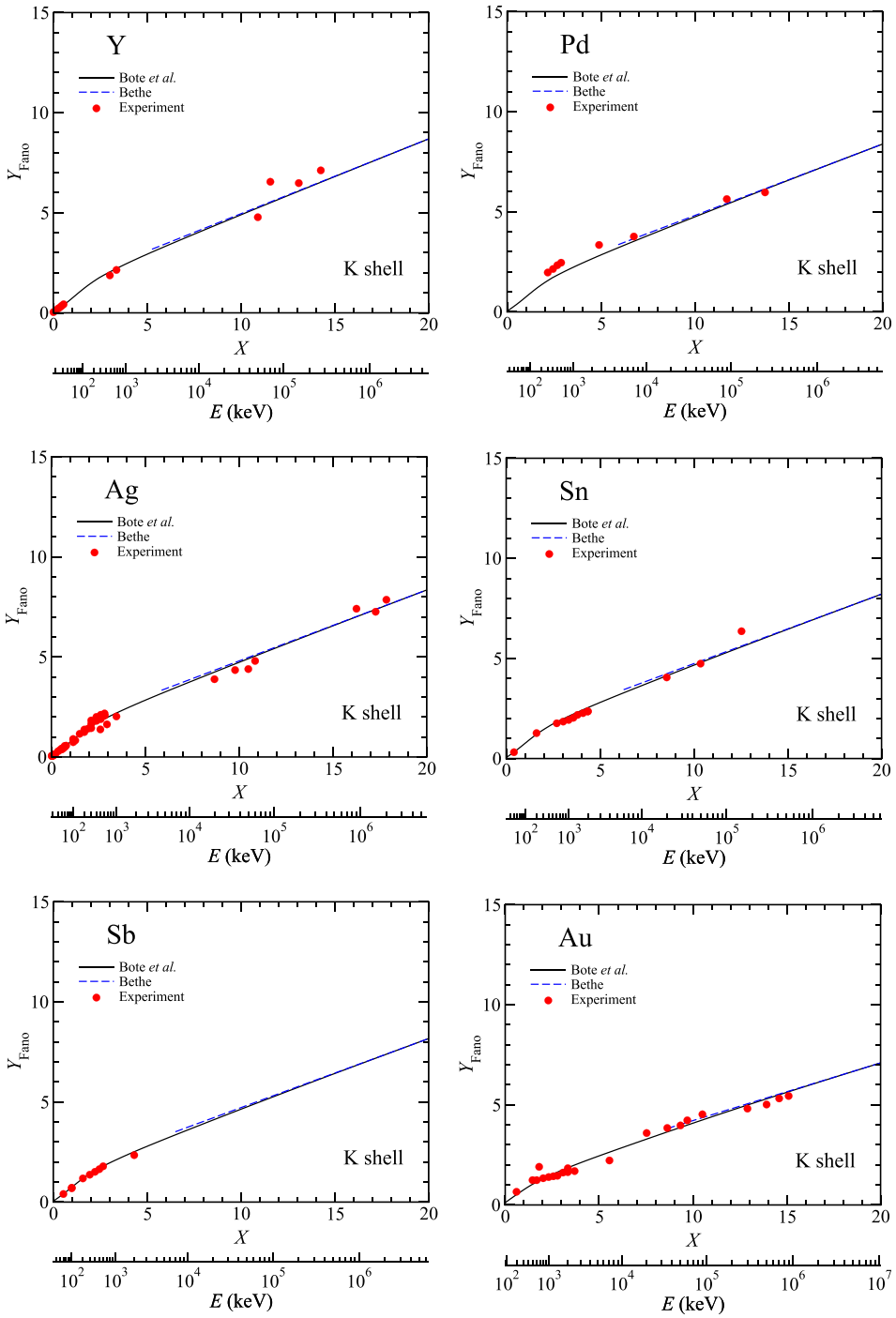

FIG. 4. Fano plots for Y, Pd, Ag, Sn, Sb, and Au; see caption to Fig. 1.

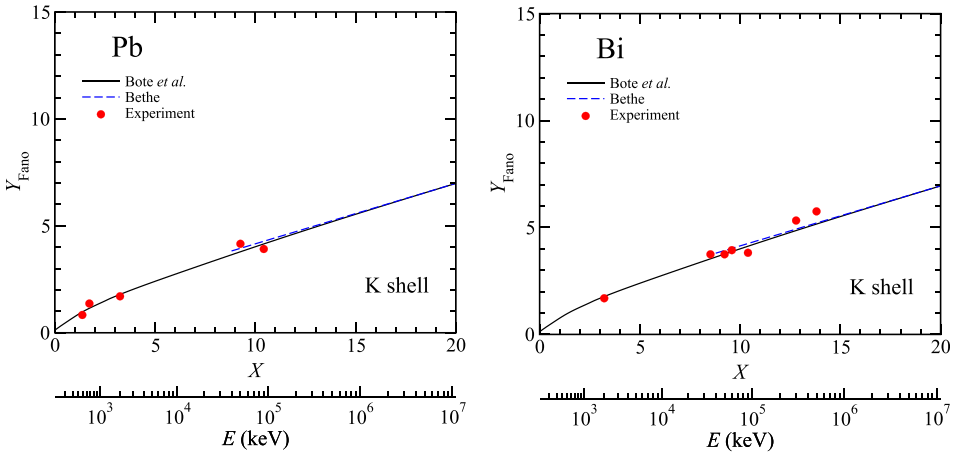

FIG. 5. Fano plots for Pb and Bi; see caption to Fig. 1.

where Z_{Lj} is the number of electrons in L-subshell j and E_{Lj} is the binding energy for these electrons. Similar equations can be written for ionization of all M subshells.

III. RESULTS

A. K-shell ionization cross sections

Figures 1–5 show Fano plots in which Y_{Fano} from Eq. (7) is plotted (solid lines) against X from Eq. (6) for C, N, O, Ne, Al, Si, Ar, Ca, Ti, Cr, Mn, Fe, Ni, Cu, Zn, Ga, Ge, Se, Y, Pd, Ag, Sn, Sb, Au, Pb, and Bi. In these plots, we have used the K-shell ionization cross sections, σ_K, calculated by Bote *et al.*[7,8] and the K-shell binding energies tabulated by Williams.[12] The abscissa also shows the corresponding electron kinetic energy, E. The Fano plots extend from the threshold for K-shell ionization ($X=0$) to $X=20$ where the maximum energy ranges from 600 MeV to 10 GeV. The solid circles in Figs. 1–5 show values of Y_{Fano} calculated from Eq. (7) with the preferred measurements of K-shell ionization cross sections of Llovet *et al.* (Tables 2 and 7 of Ref. 9) versus X from Eq. (6).

The Fano plots in Figs. 1–5 display two linear regions, as expected from the discussion of de Heer and Inokuti.[11] We will now determine values of the Bethe parameters for each linear region. The dashed lines in Figs. 1–5 show linear fits with Eq. (8) to the Y_{Fano} values from the calculated cross sections in the asymptotic high-energy regions of the Fano plots. The dashed lines have been extrapolated to a minimum energy, E_{min}, at which the deviation from the solid lines becomes 5%. Table I shows values of the Bethe parameters b_K and c_K from the fits for each element, the values of E_{min}, and the corresponding overvoltage, U_{min}. We note that no uncertainties are given for the values of b_K and c_K since values of b_K were determined from the asymptotic slopes of the Fano plots and then values of c_K from the corresponding ordinate values at $X=0$ where $Y = b_K \ln c_K$. We see that the values of b_K in Table I are about 0.52 for C, N, O, and Ne, and then gradually decrease with increasing Z to 0.281 for Bi. The values of c_K in Table I, however, increase from 5.85 for C to 116 for Bi.

The solid lines in Figs. 6–10 show expanded views of the low-energy regions of the Fano plots in Figs. 1–5, from $X=0$ to $X=4$. The dashed lines in Figs. 6–10 indicate linear fits to the Y_{Fano} values from the calculated cross sections with Eq. (8) over energy regions, E_{min} to E_{max}, where the deviations with respect to the solid lines are less than 5%. Table II shows values of the derived Bethe parameters b_K and c_K and their one-standard-deviation uncertainties from the fits for each element, the values of E_{min} and E_{max}, and the corresponding overvoltage values, U_{min} and U_{max}. We see that b_K decreases from 0.806 for C and about 0.84 for N, O, and Ne to about 0.58 for Pb and Bi. These b_K values are about 50% larger than those in Table I for the low-Z

TABLE I. Values of the Bethe parameters, b_K and c_K, derived from the linear fits with Eq. (8) in the high-energy asymptotic regions of the Fano plots with K-shell ionization cross sections in Figs. 1–5. We also show the minimum kinetic energy, E_{min}, at which the deviation of the fitted lines in the Fano plots of Figs. 1–5 becomes 5% and the corresponding value of the overvoltage, U_{min}.

Element	Z	b_K	c_K	E_{min} (keV)	U_{min}
C	6	0.512	5.85	11.7	41.0
N	7	0.527	6.25	16.1	39.3
O	8	0.524	6.37	21.9	40.3
Ne	10	0.524	6.58	36.3	41.7
Al	13	0.485	8.41	73.6	47.2
Si	14	0.475	9.03	91.2	49.6
Ar	18	0.449	11.5	199.5	62.2
Ca	20	0.435	12.8	275.4	68.2
Ti	22	0.426	14.0	374.4	75.4
Cr	24	0.418	15.1	501.2	83.7
Mn	25	0.414	15.7	566.7	86.7
Fe	26	0.411	16.2	640.7	90.1
Ni	28	0.405	17.3	806.6	96.8
Cu	29	0.403	17.8	898.1	100.0
Zn	30	0.400	18.4	1000	103.5
Ga	31	0.397	19.1	1113	107.4
Ge	32	0.394	19.9	1240	111.7
Se	34	0.388	21.3	1468	116.0
Y	39	0.374	25.7	2291	134.5
Pd	46	0.357	32.9	4105	168.6
Ag	47	0.355	34.0	4365	171.1
Sn	50	0.347	38.0	5580	191.1
Sb	51	0.345	39.5	6026	197.6
Au	79	0.288	101	31623	391.7
Pb	82	0.283	113	38019	432.0
Bi	83	0.281	116	39 204	433.1

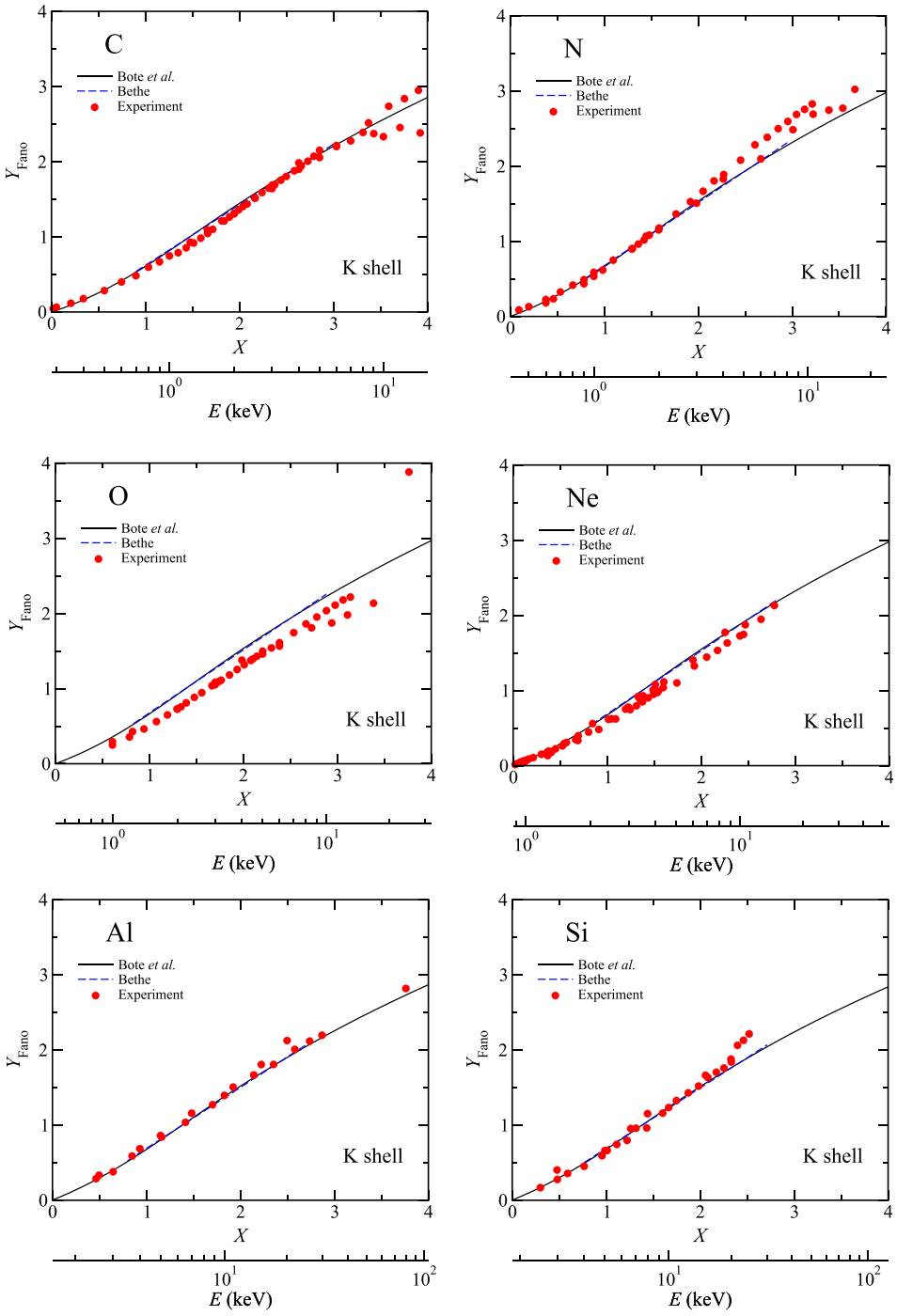

FIG. 6. Expanded view of the Fano plots for C, N, O, Ne, Al, and Si in Fig. 1 (solid lines) from $X = 0$ to $X = 4$. The abscissa also shows the electron kinetic energy, E. The dashed lines show linear fits to the Y_{Fano} values from the calculated cross sections with Eq. (8) over the energy range, E_{min} to E_{max}, where the deviations from the solid lines are less than 5%. The solid circles show values of Y_{Fano} calculated from the preferred measured K-shell ionization cross sections of Llovet *et al*. (Tables 2 and 7 of Ref. 9).

elements and about 100% larger than those in Table I for the high-Z elements. In contrast to the relatively large increases of c_K in Table I with increasing Z for the high-energy regions of the Fano plots (an increase by a factor of about 20), the values of c_K in Table II increase from 0.796 ± 0.002 for C to 1.333 ± 0.007 for Bi, an increase of less than a factor of 2. We note that the fractional uncertainties for c_K in Table II are larger than those for b_K because the uncertainties in c_K are determined from the uncertainties of both b_K and $b_K \ln c_K$ in each fit with Eq. (8).

We see from Table II that the linear regions in Figs. 6–10 range from $U_{min} \approx 1.7$ to $U_{max} \approx 8$ for the high-Z elements while the linear regions for the low-Z elements range from $U_{min} \approx 2.2$ to $U_{max} \approx 20$. The linear regions for the elements C through Ni occur, as a group, from $U_{min} = 2.3$ to $U_{max} = 15.6$. This overvoltage range is comparable with that of the 1976 Powell[4] analysis (4–24) although the lower limit of the overvoltage range found here (2.3) is about a factor of 2 smaller than in the sets of data analyzed by Powell.

Values of U_{min} for the high-energy linear regions in Table I range from about 40 for the low-Z elements to about 400 for the high-Z elements. Values of U_{max} for the low-energy linear regions in Table II range from about 20 for the low-Z elements to about 8 for the high-Z elements. The Fano plots thus change their slopes (between the two linear regions) over a narrow range of X for the low-Z elements in Fig. 1 while the slope change is much more gradual for the high-Z elements in Figs. 4 and 5.

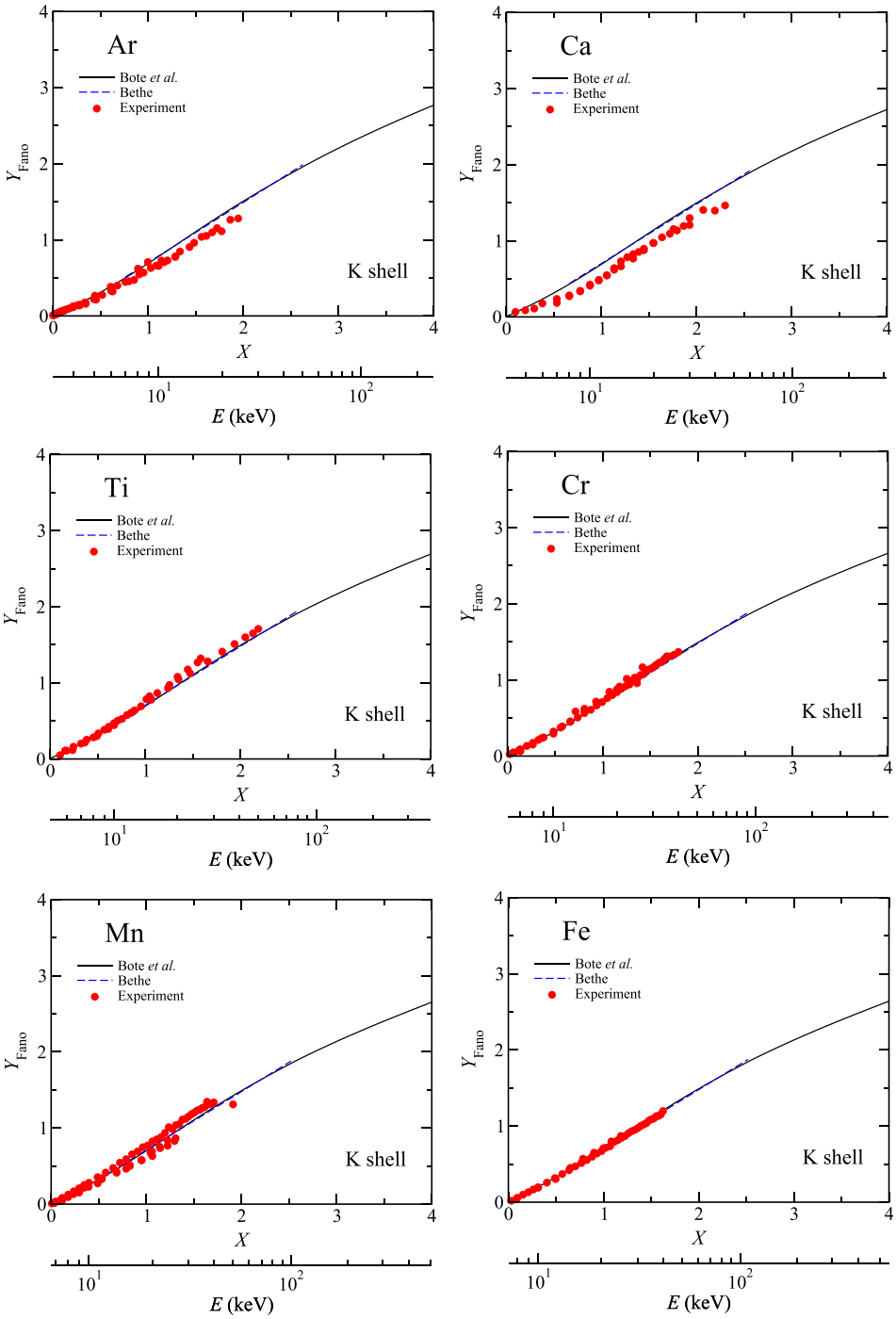

FIG. 7. Expanded view of the Fano plots for Ar, Ca, Ti, Cr, Mn, and Fe in Fig. 2 from $X = 0$ to $X = 4$; see caption to Fig. 6.

B. L-shell ionization cross sections

Figures 11 and 12 show Fano plots based on total cross sections for L-shell ionization, σ_L, in Ag, Sn, Sm, Ta, Pb, Bi, and U. As for Figs. 1–10, we have plotted Y_{Fano} from Eq. (7) versus X from Eq. (6). The solid lines show Y_{Fano} with the calculated cross sections of Bote *et al.*[7,8] and the solid circles show Y_{Fano} with the preferred measured cross sections of Llovet *et al.* (Tables 3 and 9 of Ref. 9). Values of Y_{Fano} from Eq. (7) were calculated with the average L-shell binding energies determined from the L-subshell binding energies of Williams[12] for each element that were weighted by the corresponding subshell occupancy numbers, as indicated by Eq. (11b). The abscissas in Figs. 11 and 12 also show the electron kinetic energy. As before, the Fano plots extend from the ionization threshold ($X = 0$) to $X = 20$ where the maximum energy is between 2 GeV and 5 GeV.

The Fano plots in Figs. 11 and 12 display two linear regions like those in Figs. 1–5 for K-shell ionization. We have again made linear fits to the Y_{Fano} values from the calculated cross sections with Eq. (8) in the asymptotic high-energy linear regions of each Fano plot. These fits, indicated by the dashed lines, have been extrapolated, as before, to a minimum energy, E_{min}, at which the deviations from the solid lines become 5%. Table III shows the Bethe parameters, b_L and c_L, from each fit, the values of E_{min}, and the corresponding values of U_{min}. We see that the values of b_L in Table III decrease from about 0.42 for Ag to about 0.31 for

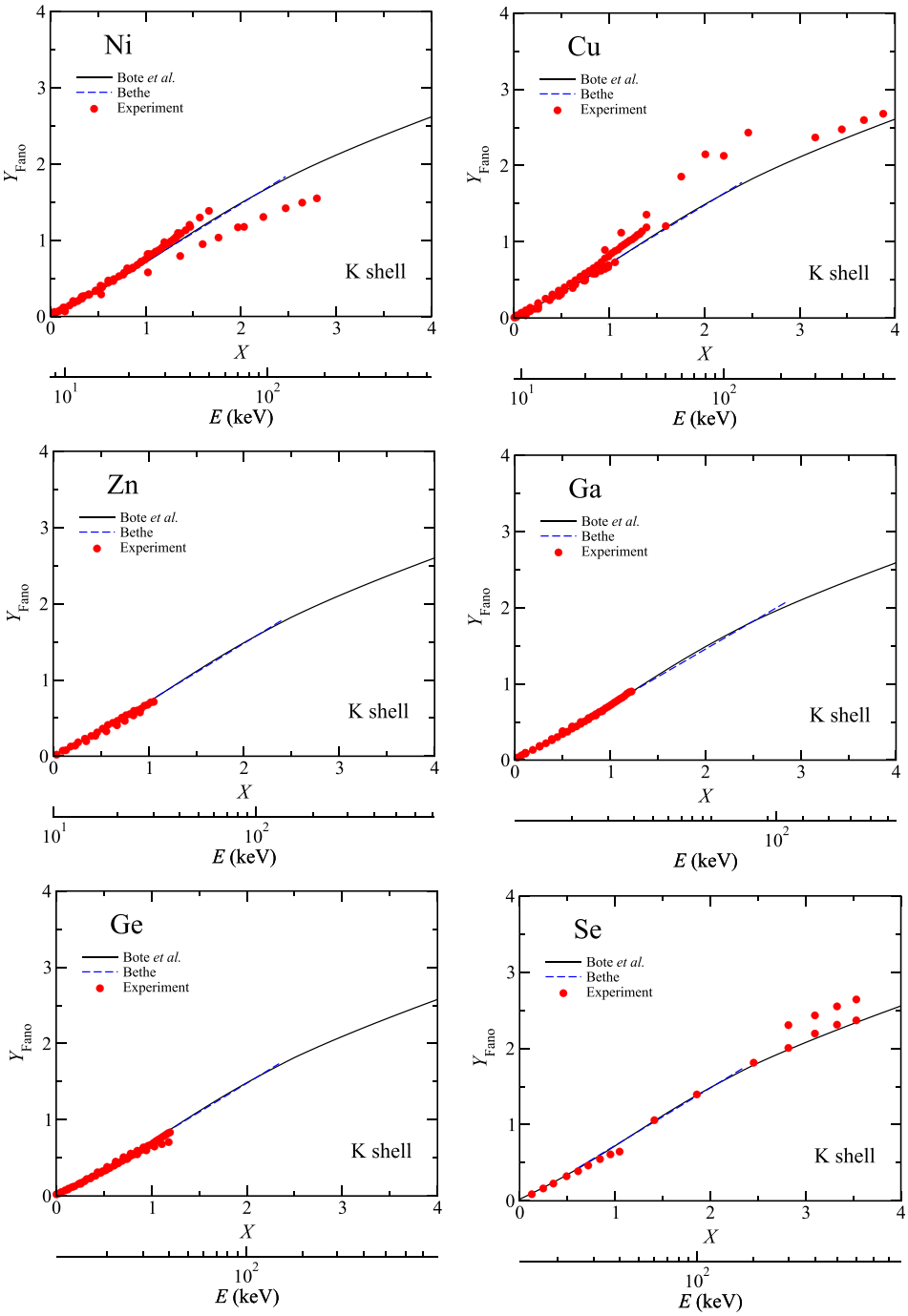

FIG. 8. Expanded view of the Fano plots for Ni, Cu, Zn, Ga, Ge, and Se in Fig. 3 from $X=0$ to $X=4$; see caption to Fig. 6.

U while the values of c_L increase from about 15 for Ag to about 70 for U. The b_L values in Table III are between 11% and 17% larger than the values of b_K in Table I that decrease from about 0.36 for Ag to about 0.28 for Bi. However, the c_L values in Table III are appreciably smaller than the c_K values in Table I which range from 34 for Ag to 116 for Bi.

Figures 13 and 14 show expanded views of the low-energy regions, from $X=0$ to $X=4$, of the Fano plots in Figs. 11 and 12. The dashed lines in Figs. 13 and 14 are, as before, linear fits to the Y_{Fano} values from the calculated cross sections with Eq. (8) over energy regions, E_{min} to E_{max}, where the deviations with respect to the solid lines are less than 5%. Table IV shows values of the derived Bethe parameters b_L and c_L and their one-standard-deviation uncertainties from the fits for each element, the values of E_{min} and E_{max}, and the corresponding overvoltage values, U_{min} and U_{max}. We see that b_L decreases from about 0.74 for Ag to 0.68 for U while c_L increases slightly from about 1.08 for Ag to about 1.30 for U. The b_L values in Table IV are larger than the corresponding values in Table III (by around a factor of 2 for Ta, Pb, Bi, and U) while the values of c_L in Table IV are more than an order of magnitude smaller than those in Table III. We also see that the values of b_L and c_L in Table IV are roughly comparable with the values of b_K and c_K in Table II for the elements Ag through Bi.

We also show Fano plots in Figs. 11 and 13 based on calculations and measurements of L_3-subshell ionization cross sections for Xe ($Z=54$). We found values of the Bethe parameters, b_{L3} and c_{L3}, in the asymptotic high-energy region in Fig. 11 to be 0.410 and 20.7, respectively, $E_{min}=292.9$ keV,

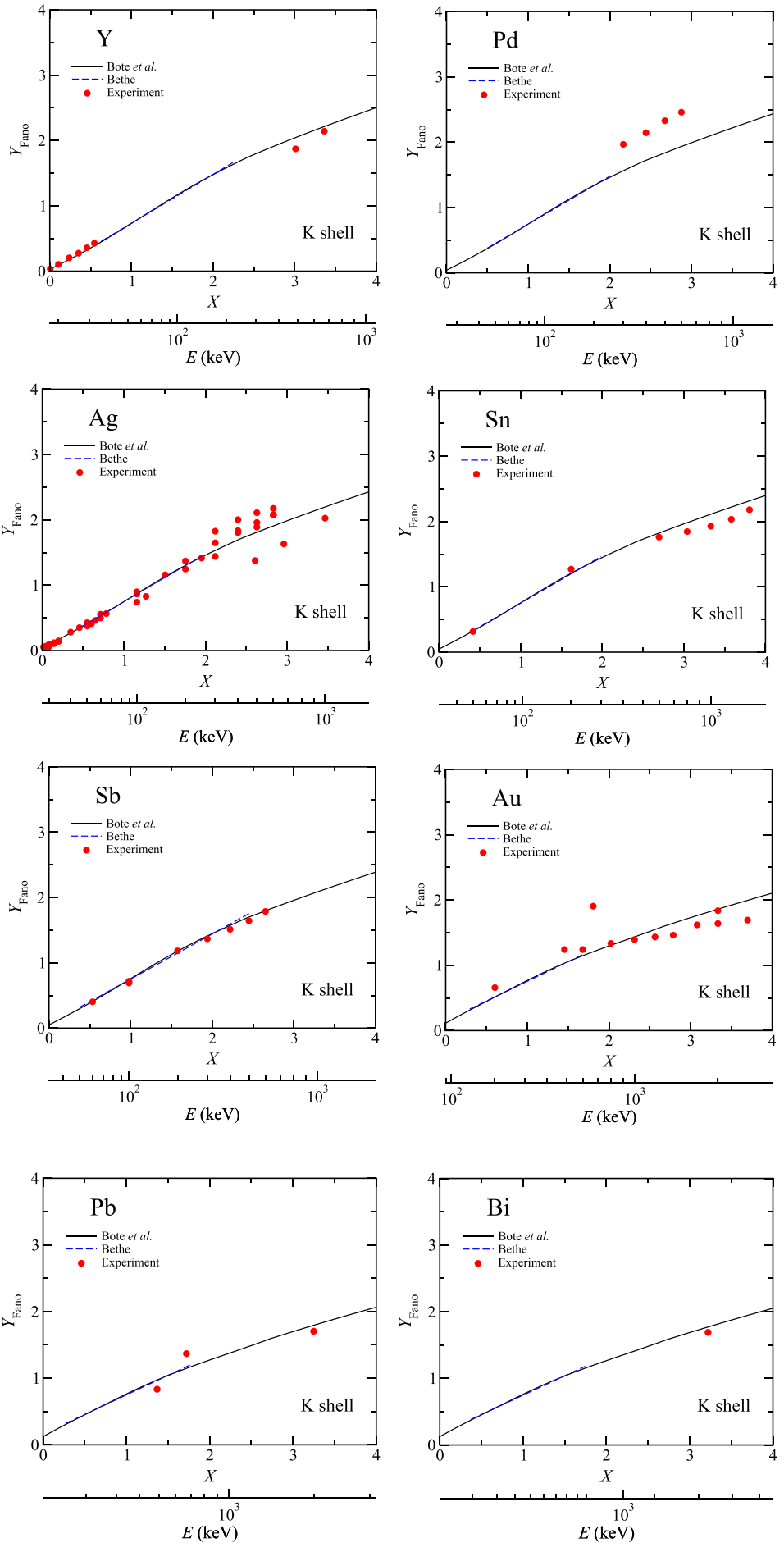

FIG. 9. Expanded view of the Fano plots for Y, Pd, Ag, Sn, Sb, and Au in Fig. 4 from $X = 0$ to $X = 4$; see caption to Fig. 6.

FIG. 10. Expanded view of the Fano plots for Pb and Bi in Fig. 5 from $X = 0$ to $X = 4$; see caption to Fig. 6.

TABLE II. Values of the Bethe parameters, b_K and c_K, and their one-standard-deviation uncertainties derived from fits with Eq. (8) in the low-energy linear regions of the Fano plots with K-shell ionization cross sections in Figs. 6–10. We also show the minimum and maximum kinetic energies, E_{min} and E_{max}, at which the deviation of the fitted lines in the Fano plots of Figs. 6–10 are less than 5% and the corresponding values of the overvoltage, U_{min} and U_{max}.

Element	Z	b_K	c_K	E_{min} (keV)	E_{max} (keV)	U_{min}	U_{max}
C	6	0.8058 ± 0.0009	0.796 ± 0.002	0.66	6.21	2.3	21.8
N	7	0.8396 ± 0.0009	0.822 ± 0.002	0.90	8.07	2.2	19.7
O	8	0.8383 ± 0.0009	0.824 ± 0.002	1.18	10.5	2.2	19.3
Ne	10	0.8412 ± 0.0009	0.832 ± 0.002	1.88	16.9	2.2	19.4
Al	13	0.812 ± 0.001	0.860 ± 0.002	3.26	28.0	2.1	17.9
Si	14	0.804 ± 0.001	0.868 ± 0.002	3.80	32.6	2.1	17.7
Ar	18	0.791 ± 0.001	0.894 ± 0.002	6.31	53.3	2.0	16.6
Ca	20	0.781 ± 0.001	0.905 ± 0.002	7.82	66.1	1.9	16.4
Ti	22	0.775 ± 0.001	0.914 ± 0.002	9.55	80.7	1.9	16.2
Cr	24	0.770 ± 0.001	0.921 ± 0.002	11.5	95.5	1.9	15.9
Mn	25	0.769 ± 0.001	0.926 ± 0.002	12.4	104.7	1.9	16.0
Fe	26	0.767 ± 0.001	0.929 ± 0.002	13.4	113.1	1.9	15.9
Ni	28	0.764 ± 0.001	0.936 ± 0.002	15.6	129.8	1.9	15.6
Cu	29	0.763 ± 0.001	0.939 ± 0.002	16.9	138.0	1.9	15.4
Zn	30	0.762 ± 0.001	0.943 ± 0.002	17.9	146.8	1.9	15.4
Ga	31	0.760 ± 0.001	0.947 ± 0.002	19.3	156.1	1.9	15.1
Ge	32	0.758 ± 0.001	0.951 ± 0.002	20.6	166.0	1.9	14.9
Se	34	0.756 ± 0.001	0.959 ± 0.002	23.3	182.0	1.8	14.4
Y	39	0.747 ± 0.001	0.981 ± 0.002	30.2	225.6	1.8	13.2
Pd	46	0.734 ± 0.001	1.016 ± 0.003	41.7	284.0	1.7	11.7
Ag	47	0.732 ± 0.001	1.021 ± 0.003	43.7	292.9	1.7	11.5
Sn	50	0.724 ± 0.002	1.038 ± 0.003	48.6	321.1	1.7	11.0
Sb	51	0.722 ± 0.002	1.043 ± 0.003	50.9	326.1	1.7	10.7
Au	79	0.601 ± 0.002	1.292 ± 0.006	138.0	670.9	1.7	8.3
Pb	82	0.587 ± 0.002	1.320 ± 0.007	146.8	702.5	1.7	8.0
Bi	83	0.581 ± 0.002	1.333 ± 0.007	153.7	713.4	1.7	7.9

and $U_{min} = 61.2$. These values are similar to the corresponding values from the total L-shell ionization cross sections for neighboring elements in Table III. For the linear fit to the low-energy region for Xe in Fig. 13, we found $b_{L3} = 0.741 \pm 0.001$, $c_{L3} = 1.165 \pm 0.003$, $E_{min} = 9.3$ keV, $E_{max} = 89.8$ keV, $U_{min} = 1.9$, and $U_{max} = 18.8$. These values are also similar to the corresponding values in Table IV derived from total L-shell ionization cross sections.

Finally, we note that the linear regions of the low-energy Fano plots in Figs. 13 and 14 range from $U_{min} = 1.5$ to $U_{max} \approx 19$ for Ag to $U_{min} = 1.9$ to $U_{max} \approx 12$ for U. We also see that the values of U_{min} in Table III for the high-energy Fano plots in Figs. 11 and 12 range from about 60 for Ag to about 162 for U. The Fano plots in Figs. 11 and 12 thus change their slopes (between the two linear regions) over a smaller range of X than for the Fano plots in Figs. 1–5.

C. M-shell ionization cross sections

Figure 15 shows Fano plots based on total cross-sections for M-shell ionization, σ_M, in Au, Pb, and Bi. As for Figs. 1–14, we have plotted Y_{Fano} from Eq. (7) versus X from Eq. (6). The solid lines show Y_{Fano} with the calculated cross sections of Bote *et al.*[7,8] and the solid circles show Y_{Fano} with the preferred measured cross sections of Llovet *et al.* (Tables 4 and 11 of Ref. 9). Values of Y_{Fano} from Eq. (7) were calculated with the average M-shell binding energies determined from the M-subshell binding energies of Williams[12] for each element that were weighted by the corresponding subshell occupancy numbers using an equation analogous to Eq. (11b) for L-shell ionization. The abscissas in Figs. 11 and 12 also show the electron kinetic energy. As before, the Fano plots extend from the ionization threshold ($X = 0$) to $X = 20$ where the maximum energy is between 1 GeV and 2 GeV.

Like Figs. 1–5, 11, and 12, the Fano plots in Fig. 15 show two linear regions. We have made linear fits to the Y_{Fano} values from the calculated cross sections with Eq. (8) in the asymptotic high-energy linear regions of each Fano plot. These fits (dashed lines) have been extrapolated to a minimum energy, E_{min}, at which the deviations from the solid lines become 5%. Table V shows the Bethe parameters, b_M and c_M, from each fit, the values of E_{min}, and the corresponding values of U_{min}. The values of b_M in Table V for Pb and Bi are about 0.53, appreciably larger than the b_L values for these elements in Table III (0.33). In contrast, the c_M values in Table V for Pb and Bi (about 8.8) are much smaller than the c_L values for these elements in Table III (about 51).

Figure 16 shows expanded views of the low-energy regions, from $X = 0$ to $X = 4$, of the Fano plots in Fig. 15. As previously mentioned, the dashed lines in Fig. 16 are linear fits to the Y_{Fano} values from the calculated cross sections with Eq. (8) over energy regions, E_{min} to E_{max}, where the deviations with respect to the solid line are less than 5%. Table VI shows values of the resulting Bethe parameters, b_M and c_M, and their one-standard-deviation uncertainties as

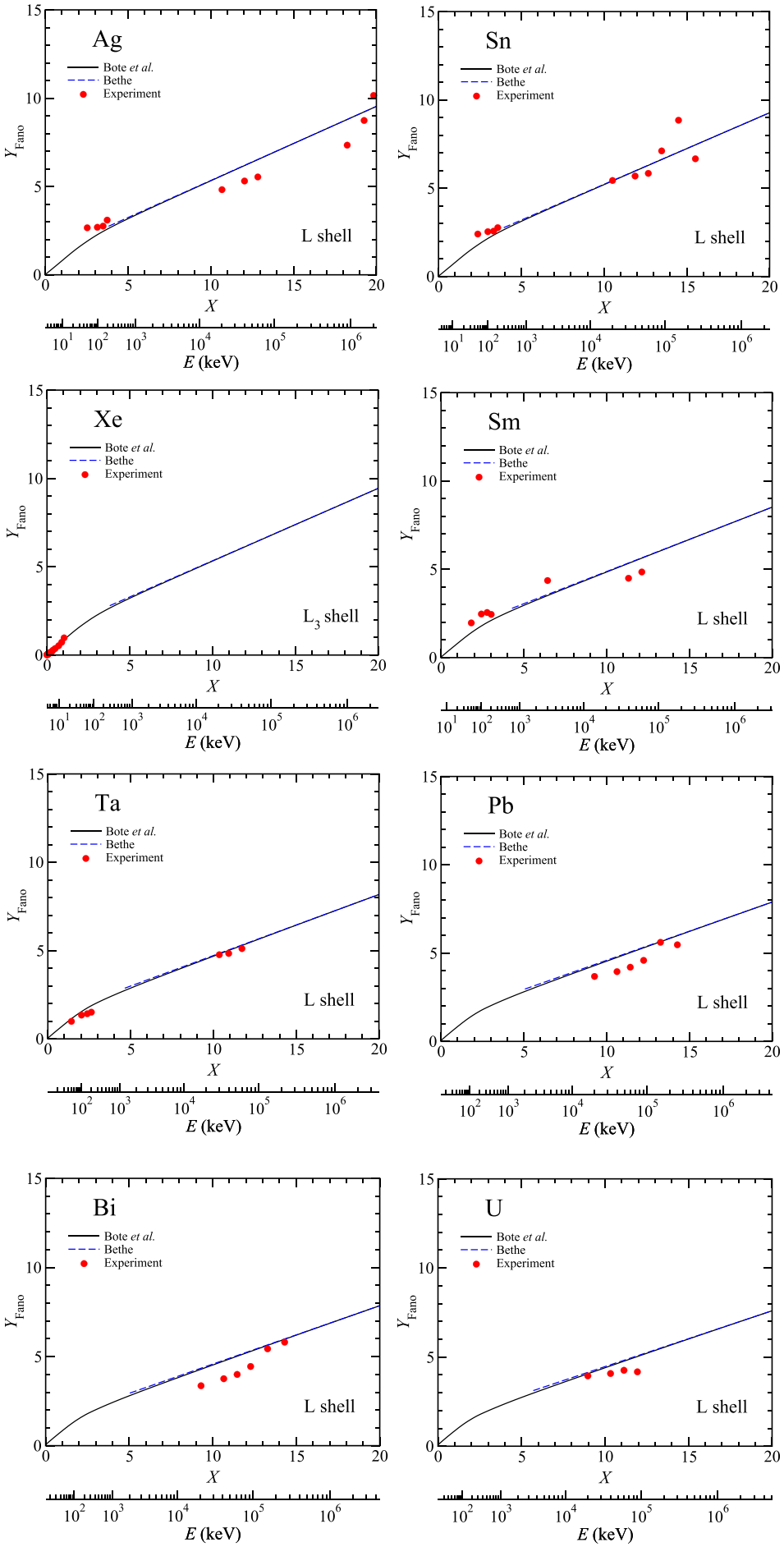

FIG. 11. Fano plots for Ag, Sn, Xe, Sm, Ta, and Pb (solid lines) based on total L-shell ionization cross sections calculated by Bote *et al.*[7,8] and Fano plot for Xe (solid line) based on the calculated L_3-subshell ionization cross sections of Bote *et al.*[7,8] In these plots, Y_{Fano} from Eq. (7) is plotted against X from Eq. (6). The abscissa also shows the electron kinetic energy, E. The dashed lines show linear fits to the Y_{Fano} values from the calculated cross sections with Eq. (8) in the asymptotic high-energy region of the Fano plots. The dashed lines have been extrapolated to a lower energy at which the deviation from the solid lines is 5%. The solid circles show values of Y_{Fano} calculated from the preferred measured total L-shell or L_3-subshell ionization cross sections of Llovet *et al.* (Tables 3 and 9 of Ref. 9).

FIG. 12. Fano plots for Bi and U; see caption to Fig. 11.

TABLE III. Values of the Bethe parameters, b_L and c_L, derived from the linear fits with Eq. (8) in the high-energy asymptotic regions of the Fano plots in Figs. 11 and 12 for Ag, Sn, Sm, Ta, Pb, Bi, and U with total L-shell ionization cross sections. We also show the minimum kinetic energy, E_{min}, at which the deviation of the fitted lines in the Fano plots of Figs. 11 and 12 becomes 5% and the corresponding value of the overvoltage, U_{min}.

Element	Z	b_L	c_L	E_{min} (keV)	U_{min}
Ag	47	0.419	15.4	202.6	57.8
Sn	50	0.405	17.9	259.0	62.9
Sm	62	0.364	29.1	621.3	87.3
Ta	73	0.346	38.6	1148	107.9
Pb	82	0.330	50.6	1848	129.4
Bi	83	0.328	52.2	1935	131.3
U	92	0.313	70.1	3114	161.7

well as the values of E_{min}, E_{max}, U_{min}, and U_{max}. We see that the values of b_M in Table VI for Pb are Bi (about 0.790) are larger than the b_L values for these elements in Table IV (0.690) while the c_M values in Table VI for the same elements (about 1.27) are essentially the same as the corresponding c_L values in Table IV (1.24).

The linear regions of the low-energy Fano plots in Fig. 16 extend from $U_{min} = 2.1$ for Au, Pb, and Bi to values of U_{max} ranging from about 32 for Au to about 29 for Bi. The values of U_{min} for the high-energy Fano plots in Fig. 15 are about 38. Unlike the L-shell Fano plots in Figs. 11 and 12, the M-shell Fano plots in Fig. 15 change their slopes between the two linear regions over a narrow range of X.

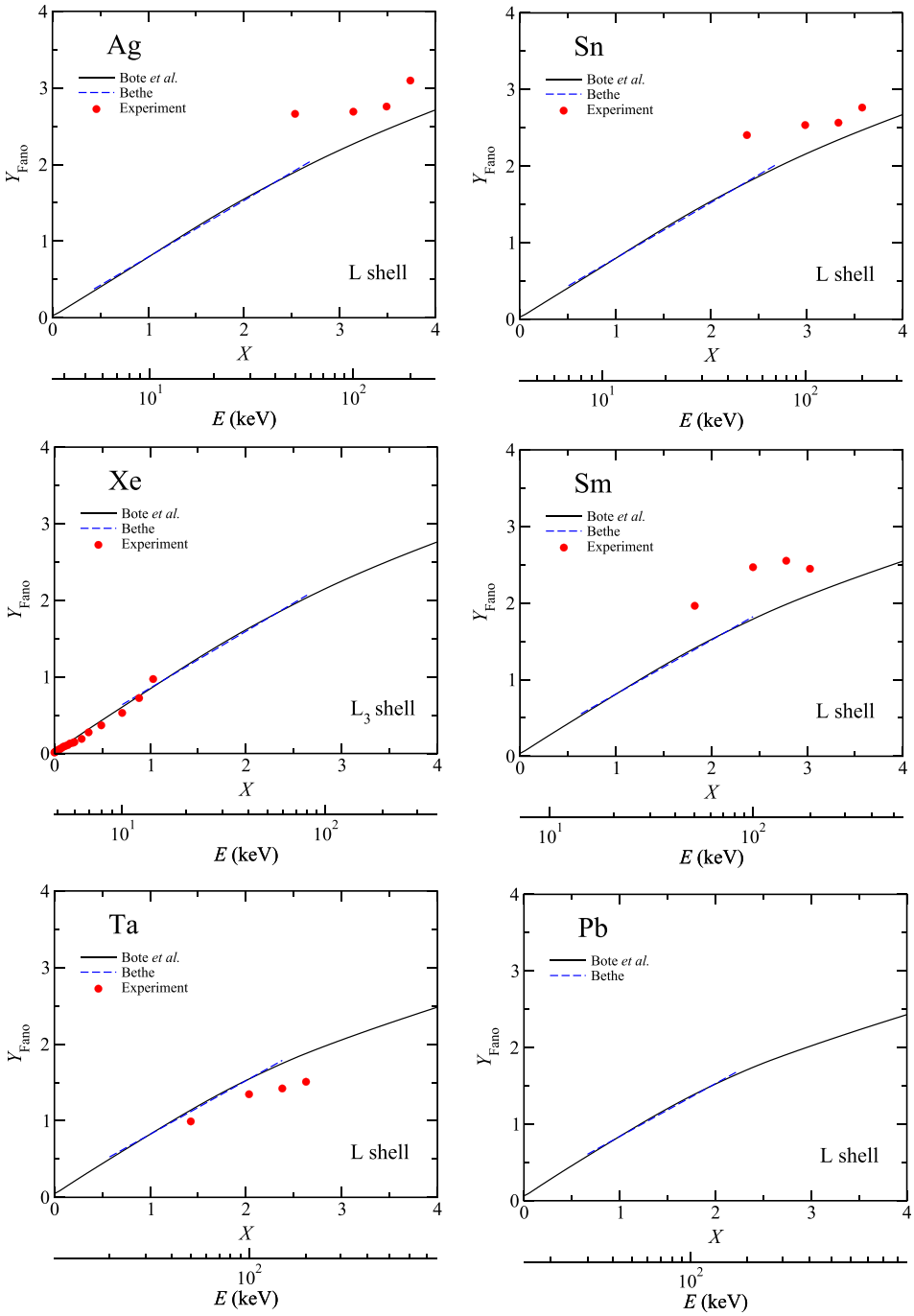

FIG. 13. Expanded view of the Fano plots for Ag, Sn, Xe, Sm, Ta, and Pb in Fig. 11 (solid lines) from $X = 0$ to $X = 4$. The abscissa also shows the electron kinetic energy, E. The dashed lines show linear fits to the Y_{Fano} values from the calculated cross sections with Eq. (8) over the energy range, E_{min} to E_{max}, where the deviations from the solid lines are less than 5%. The solid circles show values of Y_{Fano} calculated from the measured total L-shell ionization cross sections (or, for Xe, the preferred measured L_3-subshell ionization cross sections) of Llovet *et al.* (Tables 3 and 9 of Ref. 9).

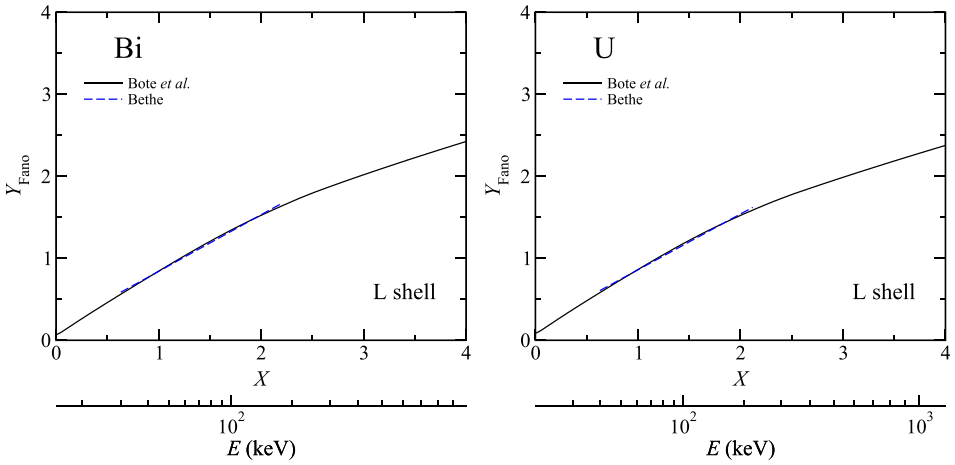

FIG. 14. Expanded view of the Fano plots for Bi and U in Fig. 12 from $X = 0$ to $X = 4$; see caption to Fig. 13.

IV. DISCUSSION

Figure 17 shows plots of the Bethe parameters b_i and c_i (i = K, L, or M) as a function of Z from fits with Eq. (8) in the high- and low-energy regions of the Fano plots in Figs. 1–16. The top panels of Fig. 17 show plots of b_i and c_i from the fits in the high-energy regions of the Fano plots shown in Figs. 1–5 for K-shell ionization, Figs. 11 and 12 for L-shell ionization, and Fig. 15 for M-shell ionization, as listed in Tables I, III, and V. We see that the values of b_K (top-left panel) decrease monotonically from about 0.52 for C, N, O, and Ne to about 0.28 for Au, Pb, and Bi. The values of b_L in the top-left panel, decreasing from about 0.41 for Ag and Sn to about 0.32 for Pb, Bi, and U, are about 15% larger than the b_K values for medium-Z (Ag and Sn) and high-Z elements (Pb and Bi). In contrast, the values of b_M in the top-left panel of Fig. 17 (about 0.53 for Au, Pb, and Bi) are about 90% larger than the b_K values for the same elements (0.28).

The values of c_K from the high-energy fits (top-right panel of Fig. 17) increase monotonically with Z from about 5.9 for C to 116 for Bi. The values of c_L, ranging from about 15 for Ag to about 70 for U, are roughly half of the values of c_K for medium-Z and high-Z elements. Finally, the values of c_M, between 7.8 and 8.9 for Au, Pb, and Bi, are about 13 times smaller than the values of c_K for the same elements.

We turn now to the values of b_i and c_i in the bottom panels of Fig. 17 that were obtained from the fits in the low-energy regions of the Fano plots shown in Figs. 6–10 for K-shell ionization, Figs. 13 and 14 for L-shell ionization, and Fig. 16 for M-shell ionization, as listed in Tables II, IV, and VI. The value of b_K (bottom-left panel) is 0.806 for C, increases to about 0.84 for N, O, and Ne, and then gradually decreases to 0.581 for Bi. The values of b_L for Ag and Sn (about 0.73) are essentially the same as the values of b_K for the same elements. However, the values of b_L for Pb and Bi (about 0.69) are around 17% larger than the values of b_K for the same elements (about 0.59). We see that the values of b_M for Au, Pb, and Bi (about 0.79) are about 34% larger than the b_K values for the same elements (about 0.59).

Overall, the b_i values from the low-energy fits range from between 0.806 for C and about 0.84 for N, O, and Ne (for K-shell ionization) to about 0.7 as a rough average of the values of b_K, b_L, and b_M for the high-Z elements. In comparison, the b_i values from the high-energy fits range from about 0.52 for C, N, O, and Ne to b_K values of about 0.28 for Au, Pb, and Bi, to b_L values of about 0.32 for Pb, Bi, and U, and to b_M values of about 0.53 for Au, Pb, and Bi. The b_K values from the low-energy fits are thus about 60% larger than those from the high-energy fits for the low-Z elements, the b_L values from the low-energy fits are roughly double those from the high-energy fits for the medium- and high-Z elements, and the b_M values from the low-energy fits are about 50% larger than those from the high-energy fits.

The values of c_K from the low-energy fits (bottom-right panel of Fig. 17) increase monotonically with Z from 0.796 for C to 1.043 for Sb but are then about 1.3 for Au, Pb, and Bi. The values of c_L range from 1.078 for Ag to 1.297 for U while the values of c_M are about 1.26 for Au, Pb, and Bi. These c_i values are appreciably less than those obtained from the high-energy fits, which can be larger by between roughly one to two orders of magnitude.

The values of b_i from the high-energy fits (top-left panel of Fig. 17) range from about 0.28 (b_K values for Au, Pb, and Bi) to about 0.53 (b_K value for N and b_M values for Au, Pb, and Bi). This range corresponds to that estimated by Bethe[1]

TABLE IV. Values of the Bethe parameters, b_L and c_L, and their one-standard-deviation uncertainties derived from fits with Eq. (8) in the low-energy linear regions of the Fano plots with total L-shell ionization cross sections in Figs. 13 and 14. We also show the minimum and maximum kinetic energies, E_{min} and E_{max}, at which the deviation of the fitted lines in the Fano plots of Figs. 13 and 14 are less than 5% and the corresponding values of the overvoltage, U_{min} and U_{max}.

Element	Z	b_L	c_L	E_{min} (keV)	E_{max} (keV)	U_{min}	U_{max}
Ag	47	0.737 ± 0.001	1.078 ± 0.002	5.29	65.1	1.5	18.5
Sn	50	0.729 ± 0.001	1.096 ± 0.002	6.51	72.4	1.6	17.6
Sm	62	0.706 ± 0.001	1.157 ± 0.003	12.6	109.6	1.8	15.4
Ta	73	0.699 ± 0.001	1.195 ± 0.004	19.3	151.4	1.8	14.2
Pb	82	0.690 ± 0.001	1.240 ± 0.004	27.1	187.6	1.9	13.1
Bi	83	0.691 ± 0.001	1.240 ± 0.004	27.5	190.5	1.9	12.9
U	92	0.681 ± 0.002	1.297 ± 0.005	37.4	229.1	1.9	11.9

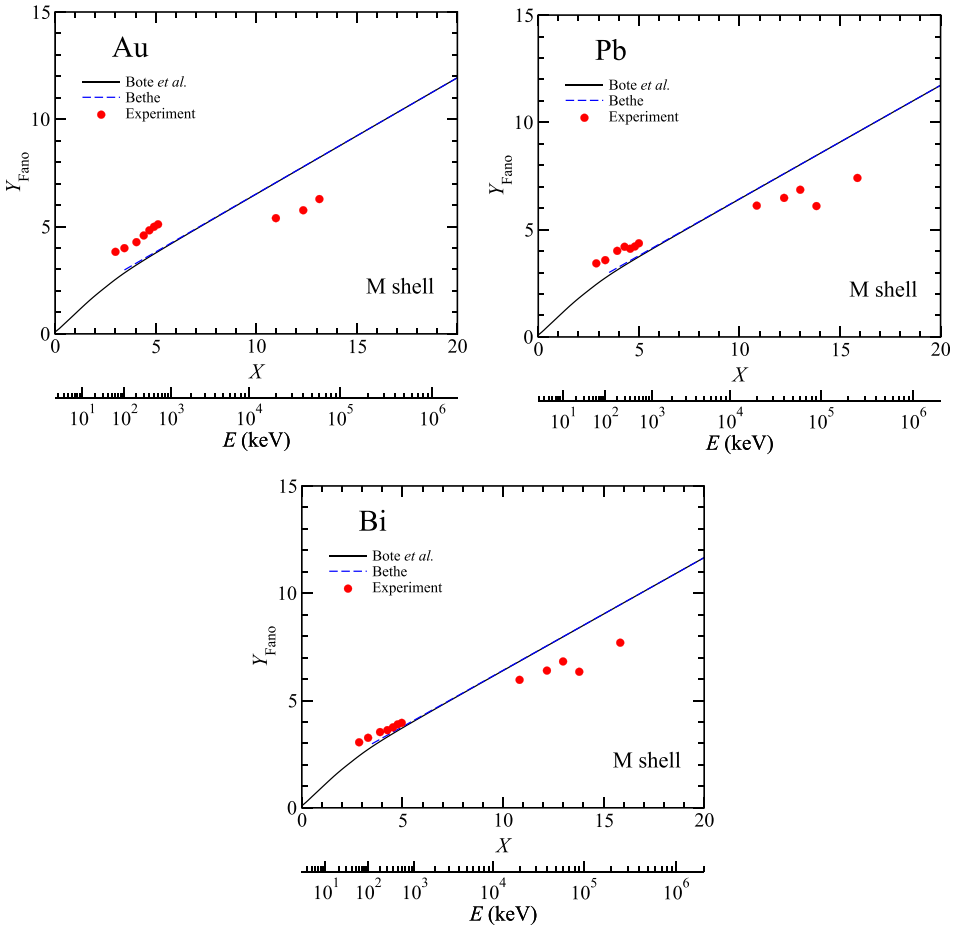

FIG. 15. Fano plots for Au, Pb, and Bi (solid lines) based on total M-shell ionization cross sections calculated by Bote *et al.*[7,8] in which Y_{Fano} from Eq. (7) is plotted against X from Eq. (6). The abscissa also shows the electron kinetic energy, E. The dashed lines show linear fits to the Y_{Fano} values from the calculated cross sections with Eq. (8) in the asymptotic high-energy region of the Fano plots. The dashed lines have been extrapolated to a lower energy at which the deviation from the solid lines is 5%. The solid circles show values of Y_{Fano} calculated from the preferred measured total M-shell ionization cross sections of Llovet *et al.* (Tables 4 and 11 of Ref. 9).

(0.2 to 0.6) with hydrogenic wave functions. However, the values of c_i from the high-energy fits (top-right panel of Fig. 17), between 5 and 116, are generally much larger than the value estimated by Bethe (about 4).

We now comment briefly on the measured cross sections for K-shell ionization shown as solid circles in Figs. 1–5. For some of the measured K-shell ionization cross sections (e.g., Si in Fig. 1; Ca, Cr, and Mn in Fig. 2; Ni, Cu, and Ge in Fig. 3; and Y, Ag, Sn, and Au in Fig. 4), there are sufficient measurements in both the low-energy and high-energy regions of the Fano plots to define adequately the two expected linear regions.[11] These two regions have not been separately observed before because cross-section measurements made in a particular laboratory were generally made over a limited range of incident electron energies. Other measured K-shell ionization cross sections (e.g., C, N, O, and Ne in Fig. 1; Ti and Fe in Fig. 2; Ga in Fig. 3; and Sb in Fig. 4) were made with incident energies that occurred only in the low-energy regions of the Fano plots. There are fewer measured cross sections for L-shell ionization in Figs. 11 and 12 and for M-shell ionization in Fig. 15 than for K-shell ionization and it is consequently harder to discern, for any one element, the existence of two linear regions in the Fano plots. The calculated ionization cross sections of Bote *et al.*[7,8] were thus invaluable not only for providing a framework for the evaluation of the measured cross sections[9] but also for clearly indicating, by the Fano plots shown here, the existence of two linear regions in the Fano plots for each element.

TABLE V. Values of the Bethe parameters, b_M and c_M, derived from the linear fits with Eq. (8) in the high-energy asymptotic regions of the Fano plots in Fig. 15 for Au, Pb, and Bi with total M-shell ionization cross sections. We also show the minimum kinetic energy, E_{min}, at which the deviation of the fitted lines in the Fano plots of Fig. 15 becomes 5% and the corresponding value of the overvoltage, U_{min}.

Element	Z	b_M	c_M	E_{min} (keV)	U_{min}
Au	79	0.541	7.79	97.0	37.5
Pb	82	0.529	8.63	111.3	38.3
Bi	83	0.526	8.92	118.4	39.2

V. SUMMARY

We analyzed the calculated cross sections of Bote *et al.*[7,8] for K-, L-, and M-shell ionization by electron impact to determine the energy ranges over which these cross sections are consistent with the Bethe equation for inner-shell ionization.[1–3] The Bethe equation is a relatively simple analytical expression with two element-specific parameters, b_i and c_i. The validity (or otherwise) of the Bethe equation for a particular set of calculated or measured ionization cross sections can be checked with a Fano plot[3] based on a linearized form of the Bethe equation. If such a plot is found to be linear for a specified energy range, the Bethe parameters, b_i and c_i, can be determined.

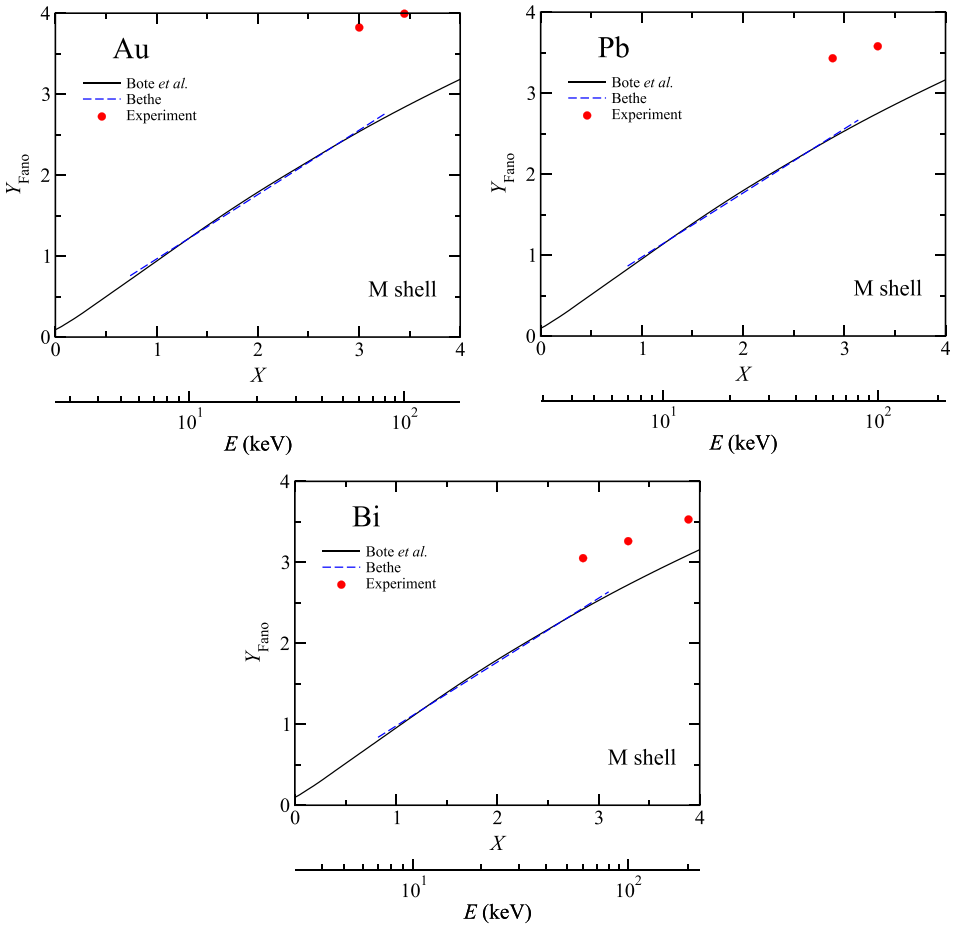

FIG. 16. Expanded views of the Fano plots for Au, Pb, and Bi in Fig. 15 (solid lines) from $X=0$ to $X=4$; see also caption to Fig. 15.

Our analysis was performed with calculated[7,8] K-shell ionization cross sections for 26 elements (C, N, O, Ne, Al, Si, Ar, Ca, Ti, Cr, Mn, Fe, Ni, Cu, Zn, Ga, Ge, Se, Y, Pd, Ag, Sn, Sb, Au, Pb, and Bi), for total L-shell ionization cross sections for seven elements (Ag, Sn, Sm, Ta, Pb, Bi, and U), with L_3-subshell ionization cross sections of Xe, and with total M-shell ionization cross sections of three elements (Au, Pb, and Bi). We have previously shown that the calculated cross sections for these elements and shells, available from the threshold energy for ionization to 1 GeV, agreed satisfactorily with sets of measured cross sections that were mutually consistent with each other and which varied with energy as expected by theory.[9]

Our Fano plots for each element and shell showed two linear regions as predicted by de Heer and Inokuti.[11] For each region, we made linear fits and obtained values of the Bethe parameters, b_i and c_i. Values of b_i for the high-energy regions were determined from the asymptotic high-energy slopes of the Fano plots after which c_i values could be calculated. The resulting straight lines were extrapolated to lower energies at which the deviations between the straight lines and each plot became 5%. The linear fits for the low-energy regions were made over energy ranges for which the deviations between the fit and each plot were also less than 5%. Our values of b_i and c_i for each element and shell are presented in Tables I–VI together with the energy ranges for which they can be used. For the high-energy fits, the minimum overvoltage ranged from about 40 for K-shell ionization of C, N, O, and Ne to around 430 for Pb and Bi while the minimum overvoltage varied from about 60 for L-shell ionization of Ag and Sn to around 160 for U; for M-shell ionization of Au, Pb, and Bi, the minimum overvoltage was around 38. For the low-energy fits, the overvoltage ranged from between around 2 and 20 for K-shell ionization of C, N, O, and Ne to between 1.7 and about 8 for Au, Pb, and Bi, and the corresponding overvoltage ranged from between 1.6 and about 18 for L-shell ionization of Ag and Sn to between 1.9 and about 12 for Pb, Bi, and U; for M-shell ionization, the overvoltage ranged between about 2 and about 30 for Au, Pb, and Bi.

We found systematic variations of b_i and c_i with Z. Values of b_K for the high-energy regions of the Fano plots decreased monotonically from about 0.52 for C, N, O, and

TABLE VI. Values of the Bethe parameters, b_M and c_M, and their one-standard-deviation uncertainties derived from fits with Eq. (8) in the low-energy linear regions of the Fano plots with total M-shell ionization cross sections in Fig. 16. We also show the minimum and maximum kinetic energies, E_{min} and E_{max}, at which the deviation of the fitted lines in the Fano plots of Fig. 16 are less than 5% and the corresponding values of the overvoltage, U_{min} and U_{max}.

Element	Z	b_M	c_M	E_{min} (keV)	E_{max} (keV)	U_{min}	U_{max}
Au	79	0.795 ± 0.001	1.238 ± 0.002	5.50	83.2	2.1	32.2
Pb	82	0.791 ± 0.001	1.263 ± 0.002	6.12	84.5	2.1	29.1
Bi	83	0.788 ± 0.001	1.274 ± 0.002	6.41	87.1	2.1	28.9

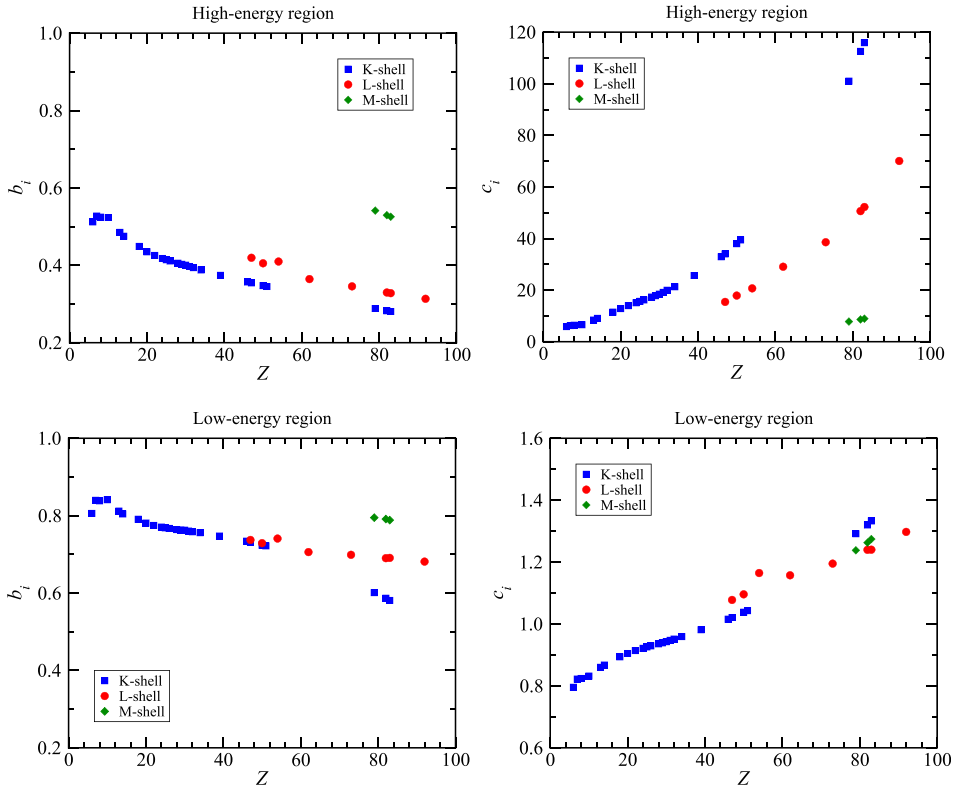

FIG. 17. Plots of the Bethe parameters b_i and c_i (i = K, L, or M) as a function of Z from fits with Eq. (8) in the high-and low-energy regions of the Fano plots in Figs. 1–16 for K-shell ionization (blue squares), L-shell ionization (red circles), and M-shell ionization (green diamonds). The left panels show plots of b_i while the right panels show plots of c_i. The top panels show the Bethe parameters from the fits in the high-energy regions of the Fano plots (Figs. 1–5 for K-shell ionization, Figs. 11 and 12 for L-shell ionization, and Fig. 15 for M-shell ionization, as listed in Tables I, III, and V). The bottom panels show the Bethe parameters from the fits in the low-energy regions of the Fano plots (Figs. 6–10 for K-shell ionization, Figs. 13 and 14 for L-shell ionization, and Fig. 16 for M-shell ionization, as listed in Tables II, IV, and VI). Error bars, corresponding to one-standard-deviation uncertainties of the Bethe parameters obtained from the fits with the low-energy Fano plots, are smaller than the size of the symbols. Values of b_{L3} and c_{L3} for Xe are also included in each panel with values of b_L and c_L, respectively.

Ne to about 0.28 for Au, Pb, and Bi while values of b_L decreased from about 0.41 for Ag and Sn to about 0.32 for Pb, Bi, and U, and b_M was about 0.53 for Au, Pb, and Bi. There were much larger variations in c_i with Z for the high-energy regions, with c_K increasing from about 5.9 for C to 116 for Bi, and c_L increasing from about 15 for Ag to about 70 for U. For the low-energy regions of the Fano plots, b_K decreased from about 0.84 for N, O, and Ne to 0.581 for Bi, the values of b_L decreased from about 0.74 for Ag to about 0.68 for U, and b_M was about 0.79 for Au, Pb, and Bi. There are much smaller variations of c_i with Z for the low-energy fits than for the high-energy fits, with c_K varying between 0.796 for C to about 1.3 for Au, Pb, and Bi, with c_L ranging between 1.078 for Ag to 1.297 for U, and with c_M about 1.26 for Au, Pb, and Bi.

Our values of b_i and c_i for the elements in Tables I–VI can be used to determine cross sections from the Bethe equation for ionization of K, L, and M shells by electron impact for the designated energy or overvoltage ranges. Similar evaluations can be made for other elements with values of b_i and c_i determined by interpolation. For many applications, however, it may be more convenient to determine these cross sections, for any element and for any energy from the ionization threshold to 100 GeV, from the empirical equations and parameters published by Bote *et al.*[8]

ACKNOWLEDGMENTS

Financial support from the Spanish Ministerio de Economía y Competitividad and the European Regional Development Fund (Project No. FPA2013-44549-P) and from the Generalitat de Catalunya (Grant No. 2014 SGR 846) are gratefully acknowledged.

[1]H. Bethe, Ann. Phys. **397**, 325 (1930).
[2]M. Inokuti, Rev. Mod. Phys. **43**, 297 (1971).
[3]U. Fano, Phys. Rev. **95**, 1198 (1954).
[4]C. J. Powell, Rev. Mod. Phys. **48**, 33 (1976).
[5]C. J. Powell, in *Electron Impact Ionization*, edited by T. D. Märk and G. H. Dunn (Springer-Verlag, Vienna, 1985), Chap. 6, pp. 198–231.
[6]C. J. Powell, in *Microbeam Analysis—1990*, edited by J. R. Michael and P. Ingram (San Francisco Press, San Francisco, 1990), p. 13–20.
[7]D. Bote and F. Salvat, Phys. Rev. A **77**, 042701 (2008).
[8]D. Bote, F. Salvat, A. Jablonski, and C. J. Powell, At. Data Nucl. Data Tables **95**, 871 (2009); erratum: **97**, 186 (2011).
[9]X. Llovet, C. J. Powell, F. Salvat, and A. Jablonski, J. Phys. Chem. Ref. Data **43**, 013102 (2014).
[10]S. Tanuma, C. J. Powell, and D. R. Penn, Surf. Interface Anal. **43**, 689 (2011).
[11]F. J. de Heer and M. Inokuti, in *Electron Impact Ionization*, edited by T. D. Märk and G. H. Dunn (Springer-Verlag, Vienna, 1985), Chap. 7, pp. 232–276.
[12]G. P. Williams, in *CRC Handbook of Chemistry and Physics*, 91st ed., edited by W. M. Haynes and D. R. Lide (CRC Press, Boca Raton, 2011), Sect. 10, pp. 221–226.